J. Fluid Mech. (2008), *vol.* 614, *pp.* 197–206.
doi:10.1017/S0022112008003352 Printed in the United Kingdom

On the limitations of Taylor's hypothesis in constructing long structures in a turbulent boundary layer

DAVID J. C. DENNIS AND TIMOTHY B. NICKELS

Department of Engineering, Cambridge University, Trumpington Street, Cambridge, CB2 1PZ, UK

(Received 24 April 2008 and in revised form 23 July 2008)

Taylor's hypothesis of frozen flow has frequently been used to convert temporal experimental measurements into a spatial domain. This technique has led to the discovery of long meandering structures in the log-region of a turbulent boundary layer. There is some contention over whether Taylor's approximation is valid over large distances. This paper presents an experiment that compares velocity fields constructed using Taylor's approximation with those obtained from particle image velocimetry (PIV), i.e. spatial data, obtained in the logarithmic region of a turbulent boundary layer.

1. Introduction

The aim of this paper is to experimentally check the extent of the accuracy of Taylor's hypothesis when applied to a turbulent boundary layer. This is done by means of an experiment which allows the production of both a spatial field, and a pseudo-spatial field using Taylor's approximation. These fields are compared both qualitatively and quantitively to assess the streamwise extent over which Taylor's approximation can be considered valid. Throughout this paper we use x, y and z as the streamwise, wall-normal and spanwise coordinates respectively, U as the streamwise velocity and u as its fluctuation.

1.1. *Long structures*

A structural element of wall-bounded turbulent flow that has recently received much attention is the "regime of very long meandering positive and negative streamwise velocity fluctuations", as described in Hutchins & Marusic (2007*a*). Figure 1, from Hutchins & Marusic (2007*a*), shows a sample of a hot-wire rake positioned at $y/\delta = 0.15$ in a $Re_\tau = 14\,380$ boundary layer flow. A very long feature can be seen meandering through the boundary layer for over 20δ (over 6.5 m at the experimental Reynolds number). This is compared with the particle image velocimetry (PIV) result shown in the inset (*b*) in figure 1, which is said to represent a snapshot of the much longer structure, (*a*). The meandering nature of this structure is said to be the reason why its true length is not apparent in one-dimensional correlations and spectra, an explanation that is quite plausible. However, spanwise hot-wire rake measurements made to investigate these structures only give instantaneous measurements at a single streamwise location. The ability to show the presence of a long meandering structure is provided by taking the fluctuating signals from the rake to reconstruct the instantaneous spanwise profile of the streamwise velocity fluctuation, and projecting it in time using Taylor's hypothesis of frozen convection to construct the structure over a long domain.

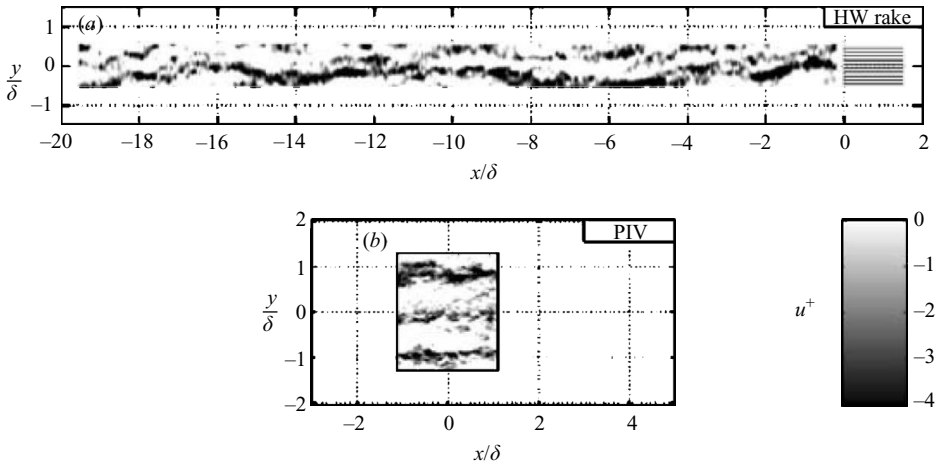

FIGURE 1. (*a*) Example rake signal at $y/\delta = 0.15$, for $Re_\tau = 14\,380$, and (*b*) PIV snapshot, from Hutchins & Marusic (2007*a*). Note their y is our z.

As well as being found in the log and lower wake regions of the turbulent boundary layer, these features are also found in pipe and channel flow (Kim & Adrian 1999; Monty *et al.* 2007). They have been found during PIV experiments (Ganapathisubramani, Clemens & Dolling 2006), and in direct numerical simulations (Ringuette, Wu & Pino Martin 2008). Long structures found using these techniques give weight to the idea that some kind of long structures do exist but do not confirm their extent in the streamwise direction. Structures have been found to span the whole streamwise extent of the velocity fields produced, however, PIV experiments have been restricted to a limited spatial region due to the constraints of the field of view of the camera, and of the difficulty in producing extensive light sheets. The largest possible streamwise extent of simultaneous measurement has so far been much less that the 20δ over which these structures are said to exist. Some aspects of long structures that have proved of interest are the proportion of the Reynolds shear stress they contain, which is found to be substantial (Ganapathisubramani, Longmire & Marusic 2003; Guala, Hommema & Adrian 2006), and their influence on the near-wall motions (Hutchins & Marusic 2007*b*; Abe, Kawamura & Choi 2004). There has also been a great deal of research regarding the relationship between long structures and hairpin vortex packets, see Adrian (2007) for an excellent review of these interesting aspects.

1.2. *Taylor's hypothesis*

In Taylor (1938) Taylor's approximation of frozen flow states that "if the velocity of the airstream which carries the eddies is very much greater than the turbulent velocity, one may assume that the sequence of changes in U at the fixed point are simply due to the passage of an unchanging pattern of turbulent motion over the point". This can be formulated (as in Townsend 1976) as

$$U(x,t) = U(x - U_c\tau, t + \tau) \tag{1.1}$$

for not too large values of τ (the time delay), and where U_c is the assumed convection velocity. This approximation is thought to be substantially accurate for boundary layer flow provided that $\overline{u^2}/U_c^2$ is small (Townsend 1976). This provides the ability to take measurements at a single streamwise location and project spatially using temporal

data, i.e. to use the measurement taken at time $t + \tau$ as an instantaneous pseudo-spatial measurement located at an offset of $U_c\tau$ from the measurement location. The small variations of τ that are possible due to the high temporal resolution of a hot wire allow for the production of a contiguous velocity field (U_c is assumed constant). However, there is some debate over the validity of Taylor's hypothesis. For example, Lin (1953) showed that it is only strictly valid if the turbulence level is low, viscous forces are negligible, and the mean shear is small (see also Lumley 1965). It is important to understand the extent to which Taylor's hypothesis can be used to accurately reconstruct flow fields in this way, as the long structures that are being found using this method could well have an important influence on our understanding of the fundamental nature of wall-bounded turbulence.

2. Experiment

The experiments were conducted using a high-speed particle image velocimetry (PIV) system in the Cambridge University Engineering Department's turbulent boundary layer water tunnel research facility. This unique facility has a $0.9\,\mathrm{m} \times 0.5\,\mathrm{m} \times 8\,\mathrm{m}$ long working section, and has been specially designed to produce thick turbulent boundary layers that may be measured with excellent spatial resolution. The experiments involved using a measurement plane parallel to the wall to obtain a velocity field in the streamwise–spanwise plane at a height above the wall at which long structures have previously been found ($y/\delta = 0.16$). The flow is tripped at the inlet to the tunnel and the measurement area is 4–5 m downstream. At this location the boundary layer thickness is $\delta = 90\,\mathrm{mm}$, the free-stream velocity is $U_\infty = 0.69\,\mathrm{m\,s^{-1}}$, the Reynolds number based on momentum thickness is $Re_\theta = 4685$, and, at the measurement height, the local mean velocity is $\overline{U} = 0.57\,\mathrm{m\,s^{-1}}$, with turbulence intensity, $u_{rms}/\overline{U} = 10\,\%$.

2.1. *Velocity fields*

The size of the measurement area was dependent on the field-of-view (FOV) of the camera. To obtain a large FOV two cameras were placed side-by-side in the streamwise direction. A single calibration plate (which covered the FOV of both cameras) was used to calibrate both the cameras. This calibration information was then used to merge the independent vector fields from each camera, creating one large vector field of approximate size $6\delta \times 3\delta$ (the longer dimension being in the streamwise direction).

Two types of fields are discussed in this paper. They are referred to as 'spatial fields' and 'Taylor fields'. Spatial fields are simply the vector fields obtained from the standard analysis of the PIV images. However, the use of a high-speed image capturing system means that there is a very short time delay between the vector fields. This meant that it was possible to take a single spanwise line of vectors from each vector field (imitating the measurement ability of a hot-wire rake) and then use Taylor's hypothesis to concatenate the lines of vectors to generate a pseudo-spatial field (similar to that shown in figure 1); the 'Taylor field'. Comparison of the Taylor field with the spatial field gives the ability to identify and quantify differences between the two fields, and hence the deficiencies of Taylor's approximation.

In this paper the focus is on the use of Taylor's hypothesis to form long meandering structures, which are obviously large-scale flow features. Therefore we may consider that the small scales are not important. To enable the examination of only the large scales in the velocity fluctuation field it is possible to use a two-dimensional Fourier

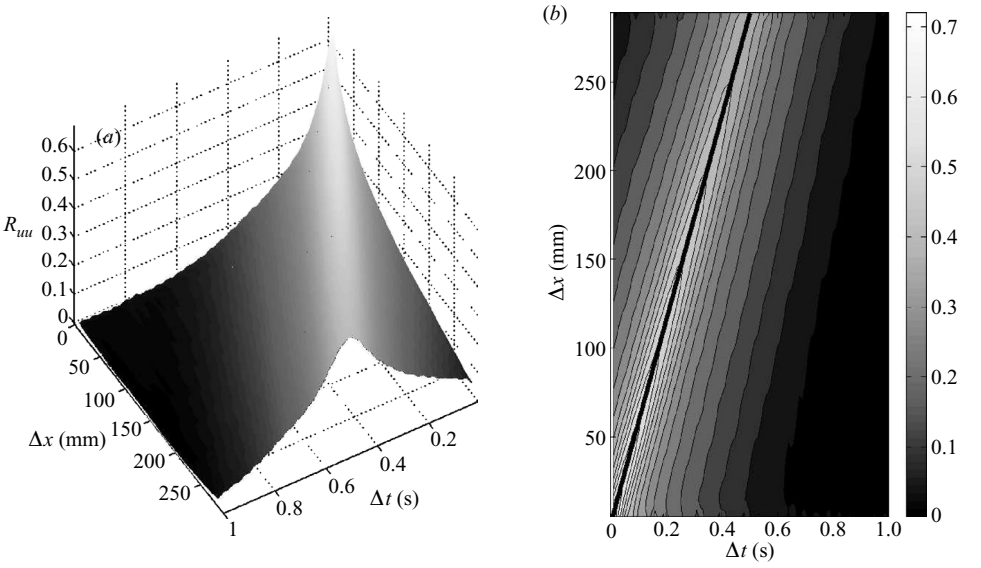

FIGURE 2. Space–time correlation; in three-dimensional (a) and two-dimensional contour plot (b). The black line shows the curve along which the change in correlation is minimized, the gradient of which is the convection velocity, $U_c = 0.58\,\mathrm{m\,s^{-1}}$.

filtering technique on the spatial and Taylor fields. This allows the removal of the small-scale motions in the fluctuating velocity fields. The filtering was performed by convolving the two-dimensional fluctuating velocity field with a two-dimensional Gaussian kernel. This cut out the high frequencies in the Fourier transform of the fluctuation field, and hence the small scales. The range of scales that are removed depends on the width of the Gaussian used. In this paper the width of the filter is defined by the standard deviation (σ) of the Gaussian in real space, given in terms of the boundary layer thickness (δ). Note that when filtered fields have been used in this paper it is explicitly stated, otherwise the unfiltered data has been used.

2.2. *Convection velocity*

The correct construction of the Taylor field is dependent on the velocity with which the flow is convected. The convection velocity (U_c in equation (1.1)) determines how far downstream it is appropriate to locate the measurements for a given time delay. It is often taken as the mean velocity at that height in the boundary layer, as in Hutchins & Marusic (2007*a*) for example. However, it was thought wise to check that this was the appropriate velocity to use. This was done by means of a space–time correlation using the streamwise velocity fields

$$R_{uu}(\Delta x, z, \Delta t) = \frac{\overline{u(x, z, t)u(x + \Delta x, z, t + \Delta t)}}{u_{rms}(z)u_{rms}(z)} \tag{2.1}$$

for a given y location. The outputs from equation (2.1) can be averaged across all values of z as the correlation is not dependent on spanwise location. Figure 2 shows the resulting space–time plot.

There are several methods that have historically been used to calculate convection velocity, see (Goldschmidt, Young & Ott 1981) for several of these. Which one is used is normally dependent on the data available. Generally the convection velocity is given by $\Delta x/\Delta t$, where Δx and Δt are changes in the spatial separation and time

delay respectively, which are chosen so as to minimize the decrease in the correlation $R_{uu}(\Delta x, \Delta t)$, (as given by equation (2.1) and plotted in figure 2), i.e. the following equation is maximized (least negative), see Fisher & Davies (1964):

$$\mathrm{d}R_{uu}(\Delta x, \Delta t) = \frac{\partial R_{uu}}{\partial \Delta t}\,\mathrm{d}\Delta t + \frac{\partial R_{uu}}{\partial \Delta x}\,\mathrm{d}\Delta x. \tag{2.2}$$

The most obvious method to calculate the convection velocity when using a pair of hot wires is to maintain a fixed streamwise separation. Therefore the second term in equation (2.2) is zero and the convection velocity is given by the Δt at which $\partial R_{uu}/\partial \Delta t$ is zero, i.e. the peak in the R_{uu} vs. Δt curve. Alternatively, using a fixed time delay, the streamwise separation is varied to maximize the correlation and hence the first term in equation (2.2) is dropped. As our PIV data allow the calculation of the two-dimensional space–time curve (figure 2), both terms can be kept. It is obvious that $|\mathrm{d}R_{uu}(\Delta x, \Delta t)|$ is minimized along the ridge of figure 2, as indicated by the black line on the contour plot. The convection velocity is simply given by the gradient of that line. In this case it is found to be $U_c = 0.58\,\mathrm{m\,s^{-1}}$, which corresponds very well with the local mean velocity ($\overline{U}/U_\infty = 0.82$, $U_c/U_\infty = 0.84$), demonstrating that the local mean is a suitable estimate for the convection velocity. It is noted here that the filtering described in § 2.1 did not have a significant effect on the convection velocity when it was calculated in this way using the filtered fields. This is perhaps not surprising since while it has been found that different wavenumbers convect at different velocities (Krogstad, Kaspersen & Rimestad 1997), this mainly affects the small scales.

3. Results and discussion

The comparison of the Taylor fields with their corresponding spatial field shows the accuracy of Taylor's hypothesis when applied to this type of flow. There are a number of ways in which the two types of field can be compared. The most obvious is to view a graphical representation of the two fields and visually spot differences between them. This method is quite informative as it gives an overall idea of the accuracy of Taylor's approximation as well as highlighting certain regions of the flow where the approximation has deficiencies (see § 3.1). There is clearly a need to quantify the accuracy of Taylor's approximation, and the correlation of the Taylor field with the spatial field (§ 3.2) has been used to show the relationship between the spatial and Taylor fields, and the way in which it varies with downstream distance. This allows some deductions and comments to be made regarding the extent to which Taylor's approximation is valid.

3.1. *Visual comparison*

As the long structures that are the focus of this paper are characterized by patterns in the streamwise velocity fluctuations, it is most pertinent to visually examine the plots of streamwise velocity fluctuations of the spatial and Taylor fields side by side. An example of a comparison of the spatial and Taylor fields is shown in figure 3. We can immediately see many similarities between them; they are a reasonably good match. However, it is possible to identify distinct regions of difference between them. Some of these areas are highlighted by the rings and boxes in figure 3. The differences between the two fields can be categorized into three types:

(i) Differences that fall under the first category are indicated in figure 3 by the boxes. These are major differences in the two fields where a large-scale feature is seen to be present in one field and entirely absent from the other. In figure 3 the smaller

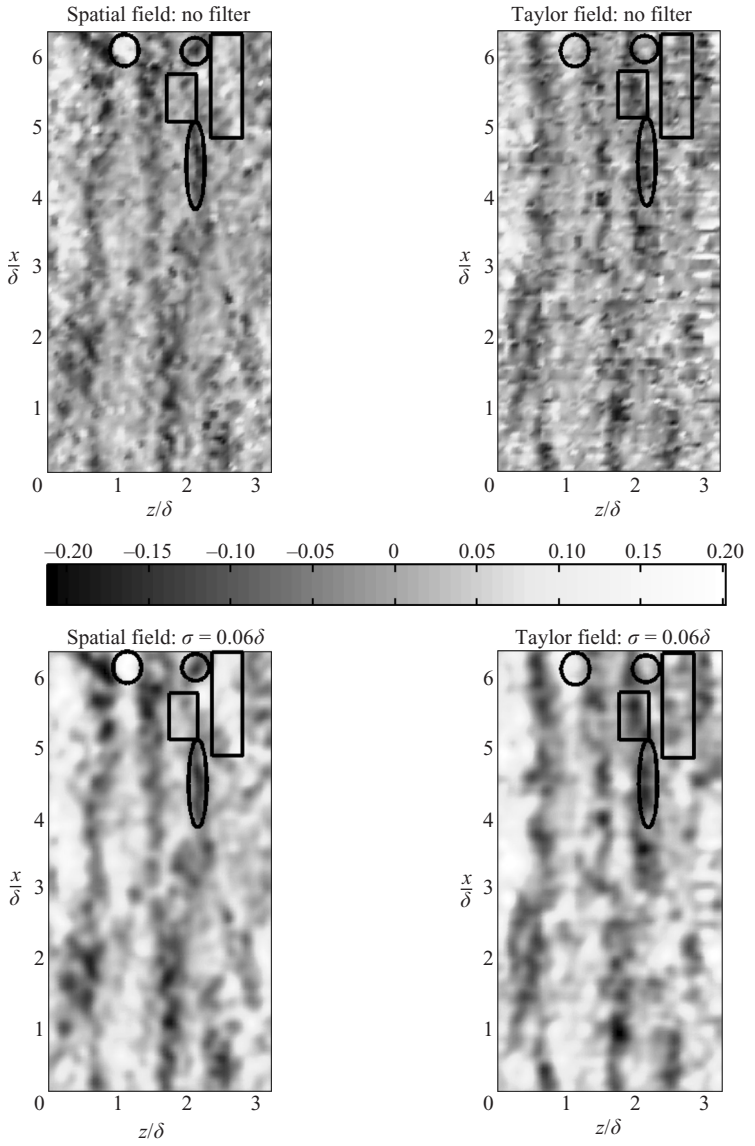

FIGURE 3. Comparison of the spatial and Taylor fields of the streamwise velocity fluctuation over a $6\delta \times 3\delta$ area: unfiltered (top) and filtered (bottom). (Colourmap scale is in $\mathrm{m\,s^{-1}}$).

box highlights a low-speed region that is found in the Taylor field but not in the spatial field. The larger box is a high-speed region present in the spatial field and not the Taylor field. From the examination of many comparisons it is evident that errors of this nature are found with reasonable frequency (generally 1 or 2 per field). It is also possible to assert that the vast majority of these type of errors occur in the latter parts of the field, generally $x/\delta > 4.5$, and that they are normally between 0.5δ and 1.5δ in streamwise extent.

(ii) Differences of the second type have been marked by rings/ellipses in figure 3. These are also large-scale differences but here it is possible to see, by examining the surrounding field, that they may be out of place in the Taylor field when compared

to the spatial field, as opposed to simply absent. These types of differences are considerably harder to spot because they are often subtle and the offset is not always very large. However, figure 3 shows clearly that the flow features seen to be enclosed by the rings in the spatial field are not so enclosed in the Taylor field. It is possible to offer an explanation for these differences. As we can see from the spatial field it is commonplace for the long structures to meander in space. The pertinent difference between the Taylor and spatial fields is that the spatial fields are instantaneous, whereas the Taylor fields are pieced together from a series of time-stepped measurements. Therefore the fact that structures appear to have meandered differently in the Taylor field when compared to the spatial field implies that the long structures meander in time as well as space. It is no surprise at all that Taylor's approximation fails to capture the meandering of structures in time, as Taylor's hypothesis assumes structures to be 'frozen' in time (basically they are assumed to be rigid objects convecting with speed U_c). The differences identified in this category occur in the latter part ($>3.5\,\delta$) of the field.

(iii) The third type of differences are the minor variations that are present throughout the whole extent of the field. These are mostly seen as subtle differences in the magnitude of the velocity fluctuation, rather than being in the pattern itself, so are hard to pick out individually, and not particularly important if we are considering long structures.

Shown in lower half of figure 3 are the spatial and Taylor fields that have been filtered as described in § 2.1. It is clear that some of the smaller scales have been removed, as is the intention of the filtering. Along with the small scales, some of the errors of category (iii) have also gone, although clearly some still remain. However, it is also plainly obvious that the large-scale differences highlighted by the rings and boxes (and described above) are still present in the filtered fields.

It is possible to see from the example shown in figure 3 a situation where the Taylor field could lead to incorrect interpretation regarding the long structures. The region of low velocity that starts at ($z/\delta = 2.2$, $x/\delta = 3$) and continues to ($z/\delta = 2$, $x/\delta = 6.3$) in the Taylor field is not present as a whole in the spatial field, although it is in parts.

One would obviously expect the accuracy of Taylor's approximation to deteriorate as it is used to project over increasingly large distances, which is highlighted by the fact that the differences described above occur more frequently with increasing x/δ. It is necessary to quantify both the difference between the spatial and Taylor fields, and how this difference varies with increasing downstream projection.

3.2. *Correlation of Taylor and spatial fields*

The correlation of the Taylor field with its corresponding spatial field has been used as a quantitative measure of the similarity between the two fields. Each pair of realizations is correlated, and the average correlation over all realizations is calculated. This two-dimensional correlation map is then averaged in the spanwise direction as the correlation is only expected to vary with streamwise distance, not spanwise. The correlation is shown in figure 4, with the correlation value calculated as given by the following equation, where all values are *local* and the subscripts S and T indicate the spatial and Taylor fields respectively:

$$R_{u_S u_T} = \frac{\overline{u_S u_T}}{\sqrt{\overline{u_S^2}}\sqrt{\overline{u_T^2}}}. \tag{3.1}$$

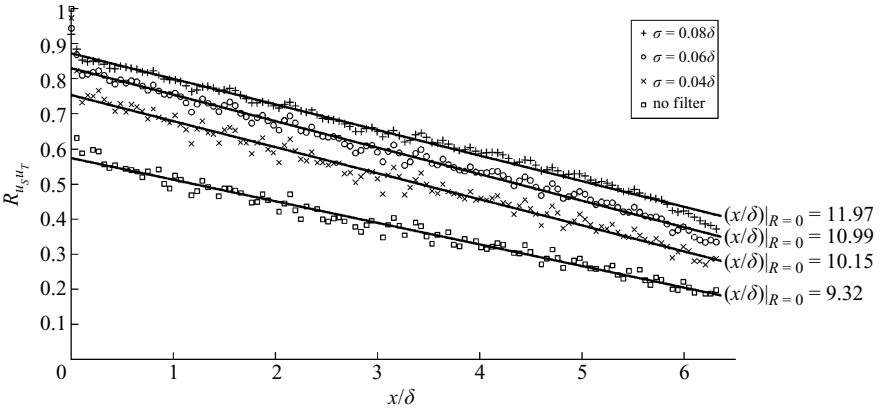

FIGURE 4. The correlation of the Taylor and spatial fields for different levels of filtering.

Figure 4 shows different curves for different levels of filtering. These will be discussed later; initially we will concentrate on the unfiltered results (squares). The curve shows an approximately linear decrease in the accuracy of Taylor's approximation with streamwise projection distance. The value of the correlation ($R_{u_S u_T}$) falls to 0.19 at the greatest extent of the FOV ($\approx 6.3\delta$). Projecting the trend forwards using a linear fit indicates that the correlation value would drop to zero at $x/\delta = 9.32$. However, this linear trend cannot continue indefinitely, and this value should be taken simply as an indicator of the rate of decay of the correlation. Considering the observations from the visual comparison (§ 3.1) the most likely reason for the drop in the correlation is that the structures are distorting in time.

By definition the correlation is equal to 1.0 at $x/\delta = 0$. The next point on the curve (i.e. the first point that uses Taylor's approximation) shows a correlation value of 0.63. This implies that a large inaccuracy is immediately introduced when Taylor's approximation is employed. To a certain extent, this is unexpected, because the perceived accuracy of the Taylor fields we examined visually was very high over very short displacements (see § 3.1). However, when we consider the inaccuracies that we are likely to notice by eye, i.e. large-scale differences, it is less surprising to discover that we had not fully appreciated the errors over short distances. Now consider the scale of the features that we are particularly interested in: the large-scale motions. Fourier filtering, described in § 2.1, can be used to remove the small-scale motions from the velocity fluctuation fields before they are correlated, therefore removing the effect of the smaller scales on the correlation value. The results of this procedure for varying levels of filtering are shown in figure 4. (Note that the higher the value of σ the greater the extent of the filtering, i.e. the *more* scales are cut out.)

From figure 4 it is apparent that filtering out the small scales increases the correlation value across the whole range of x/δ. Indeed, the more extreme the filtering the greater the correlation. The filters have been defined by the standard deviations of the Gaussian in terms of δ, $\sigma/\delta = 0.04$, 0.06 and 0.08. These correspond to Gaussian total widths (6σ) of 0.24δ, 0.36δ and 0.48δ respectively. According to the two-point correlation of the streamwise velocity fluctuation in Hutchins & Marusic (2007*a*), the spanwise width of long structures at approximately the same height is 0.4δ. Therefore increasing the width of the filter any more would start to have an effect on the long structures themselves.

It should be noted that the correlation value at $x/\delta = 0$ is not equal to 1.0 for the filtered results; this is due to the whole field filtering contaminating the first row of values, meaning that the initial values of the spatial and Taylor fields are no longer identical. There are also the usual 'end effects' associated with Fourier filtering, which have been mitigated by the use of zero-padding, but some very small effect does remain.

The significant increase in the correlation with filtering adds some weight to the idea that the initial drop-off is predominantly due to the small scales, especially as the increase is most apparent at small x/δ where small scales will have the largest effect. This is shown by the small increase in gradient in the filtered fields when compared to the unfiltered field. The projections at which $R_{u_S u_T} = 0$ are given on figure 4, and there is a clear increase with filtering.

It is possible to argue that, if we are only interested in the large-scale motions, then we can use Taylor's approximation over a greater projection distance. Indeed, it would be possible to routinely filter the velocity fields that have been produced using Taylor's approximation in this way, so that the obvious small-scale errors were removed. The correlation was also performed with only the Taylor field filtered (as the Taylor field would be the only one available in a normal experiment). This increased the correlation significantly, although not quite as much as when both fields are filtered.

It is not possible to state a universal limit on the use of Taylor's hypothesis, since this will vary depending on the experiment. The information here, however, should provide some guidance.

Finally, we note that although it does appear to be advisable to limit the projection distance over which Taylor's hypothesis is used, if the experiment has some streamwise extent (e.g. PIV), then it is possible to use Taylor's approximation to project both forwards and backwards in time by the limit of the projection distance, as was demonstrated in Dennis & Nickels (2007). This effectively doubles the length of possible projection distance. The spatial field can then be sandwiched between the two Taylor fields, giving a reliable field of some considerable length.

4. Conclusions

This experiment has demonstrated the accuracy of Taylor's approximation when applied to a turbulent boundary layer for projection distances up to 6δ. The production of both the spatial field and the corresponding field created using Taylor's approximation has enabled direct qualitative and quantitative comparisons to be made. A visual examination of the two fields shows a striking similarity, although some significant large-scale differences are also evident. The vast majority of the differences occur in the latter half of the field. A quantitative analysis was performed by correlating the appropriate spatial and Taylor fields. It was found that there was a strong correlation between the two fields, and this correlation decreased approximately linearly with projection distance. It has been proposed that a significant proportion of the error between the two fields is due to small-scale motions that are not maintained in time, and as such, are a source of consistent error. A method of Fourier filtering has been used to filter out the small scales. The correlation was found to increase significantly when the filtered fields were used. This suggests that Taylor's approximation can be used to a greater extent if it is only the large scales that are of interest. However, care must be taken since excessive filtering will distort the actual structures and lead to erroneous results.

REFERENCES

Abe, H., Kawamura, H. & Choi, H. 2004 Very large-scale structures and their effects on the wall shear-stress fluctuations in a turbulent channel flow up to $Re_\tau = 640$. *Trans. ASME: J. Fluids Engng* **126**, 835–843.

Adrian, R. J. 2007 Hairpin vortex organization in wall turbulence. *Phys. Fluids* **19**, 041301.

Dennis, D. J. C. & Nickels, T. B. 2007 On the use of Taylor's hypothesis in constructing long structures in wall-bounded turbulent flow. In *Advances in Turbulence XI: Proc. 11th EUROMECH European Turbulence Conference, June 25–28, Porto, Portugal* (ed. J. M. L. M. Palma & A. Silva Lopes), pp. 236–238. Springer.

Fisher, M. J. & Davies, P. O. A. L. 1964 Correlation measurements in a non-frozen pattern of turbulence. *J. Fluid Mech.* **18**, 97–116.

Ganapathisubramani, B., Clemens, N. T. & Dolling, D. S. 2006 Large-scale motions in a supersonic turbulent boundary layer. *J. Fluid Mech.* **556**, 271–282.

Ganapathisubramani, B., Longmire, E. K. & Marusic, I. 2003 Characteristics of vortex packets in turbulent boundary layers. *J. Fluid Mech.* **478**, 35–46.

Goldschmidt, V. W., Young, M. F. & Ott, E. S. 1981 Turbulent convective velocities (broadband and wavenumber dependent) in a plane jet. *J. Fluid Mech.* **105**, 327–345.

Guala, M., Hommema, S. E. & Adrian, R. J. 2006 Large-scale and very-large-scale motions in turbulent pipe flow. *J. Fluid Mech.* **554**, 521–542.

Hutchins, N. & Marusic, I. 2007*a* Evidence of very long meandering features in the logarithmic region of the turbulent boundary layers. *J. Fluid Mech.* **579**, 1–28.

Hutchins, N. & Marusic, I. 2007*b* Large-scale influences in near-wall turbulence. *Phil. Trans. R. Soc. Lond.* A. **365**, 647–664.

Kim, K. C. & Adrian, R. J. 1999 Very large-scale motion in the outer layer. *Phys. Fluids* A **11**, 417–422.

Krogstad, P. A., Kaspersen, J. H. & Rimestad, S. 1997 Propagation velocity of perturbations in turbulent channel flow. *Phys. Fluids* A **10**, 949–957.

Lin, C. C. 1953 On Taylor's hypothesis and the acceleration terms in the Navier-Stokes equation. *Q. Appl. Maths* **10**, 295–306.

Lumley, J. L. 1965 Interpretation of time spectra measured in high-intensity shear flows. *Phys. Fluids* **8**, 1056–1062.

Monty, J. P., Stewart, J. A., Williams, R. C. & Chong, M. S. 2007 Large-scale features in turbulent pipe and channel flows. *J. Fluid Mech.* **589**, 147–156.

Ringuette, M. J., Wu, M. & Pino Martin, M. 2008 Coherent structures in direct numerical simulation of turbulent boundary layers at Mach 3. *J. Fluid Mech.* **594**, 59–69.

Taylor, G. I. 1938 The spectrum of turbulence. *Proc. R. Soc. Lond.* A **164**, 476–490.

Townsend, A. A. 1976 *The Structure of Turbulent Shear Flow*, 2nd edn. Cambridge University Press.